Journal of Material Cycles and Waste Management
https://doi.org/10.1007/s10163-018-0770-1

ORIGINAL ARTICLE

Mechanical properties and microstructure of cement mortars incorporating Cd-zeolitized fly ash

J. D. Monzón[1] · A. M. Pereyra[1,2] · M. R. Gonzalez[2] · R. L. Zerbino[3] · Elena I. Basaldella[2]

Received: 29 August 2017 / Accepted: 27 July 2018

Abstract
A solid enriched with NaA zeolite was synthesized from a coal fly ash, and the so-obtained zeolitized material was used as ion exchanger for purifying aqueous solution containing cadmium cations. Mechanical strengths and drying shrinkage measured on cement mortars containing not more than 10 wt% of the zeolitized product showed that the cement properties remained unaltered, being similar to those corresponding to mortars where non-zeolitized starting fly ash was used in the mortar formulation. SEM analyses of fractured mortars show zeolitized fly ash particles strongly anchored inside the microstructure, the particle surfaces being densely covered by hydration products. To analyze the viability of final disposal for the cadmium sludge obtained after ion exchange, a leaching test was performed on cement pastes containing 10 wt% of cadmium-exchanged zeolite (Cd-ZFA10) showing that the present methodology is an effective procedure for the immobilization of the heavy metal.

Keywords Heavy metal immobilization · Zeolites · Fly ash · Portland cement mortars · Mechanical properties

Introduction

Heavy metals are becoming one of the most serious environmental problems because of their accumulation in aquatic organisms and in agricultural crops with severe implications for the food chain. The main heavy metals from anthropogenic sources, such as industrial activities, are chromium, nickel, zinc, cadmium, copper, lead, and mercury. They are directly discharged into the environment; their persistence and null biodegradability affect the air, soil and water [1].

Particularly, cadmium has been classified as possible carcinogen and nephrotoxicant by US EPA. Cadmium enters the human body through vegetables, animal products and drinking water, exposing human health to severe risks. The fertilizer industry and the mining and metallurgical (nonferrous) sectors contribute significantly to cadmium pollution [2].

✉ Elena I. Basaldella
eib@quimica.unlp.edu.ar

[1] Universidad Tecnológica Nacional, 60 y 124, 1900 La Plata, Argentina

[2] CINDECA (CONICET-CIC-UNLP), 47 No. 257, B1900AJK La Plata, Argentina

[3] CONICET-Fac. Ing. UNLP, LEMIT, 52 entre 121 y 122, B1900AYB La Plata, Argentina

A wide range of treatments for removing heavy metals in aqueous solution is known. Among them, chemical precipitation is widely used in the industry because of its low cost and effectiveness. Other technologies based on an ion-exchange process, adsorption and membrane filtration have been developed and thoroughly studied for the treatment of hazardous metal wastewater.

Cadmium removal from aqueous solution by many different materials has been studied. Recent developments propose adsorbent materials such as fluor-hydroxyapatite composites [3], copper oxide nanoblades [4], sulfonated magnetic nanoparticle [5], dithiocarbamate functionalized pyrrole-based terpolymers [6], polyethylenimine-functionalized mesocellular silica foam [7], TMU-16-NH_2 metal organic framework [8], natural clays [9, 10], synthetic polymers [11], among others.

Synthetic zeolites exhibit good ion-exchange capacities for heavy metal cation removal under different experimental conditions at laboratory scale [12–14]. Zeolite could be synthesized from conventional raw materials or using alternative sources of SiO_2 and Al_2O_3 such as some industrial wastes generated by different energy production processes [15–20]. In particular, the synthesis of zeolites from fly ash is receiving increasing attention since it allows obtaining a product with valuable technological applications using

Published online: 06 August 2018

inexpensive raw materials and a concomitant reuse of a difficult disposal waste.

More than 600 million tons of fly ash are produced annually around the world [21, 22]. A percentage is used as road bases to improve lands and to treat mud in residual waters [23, 24]. Statistical data confirm that approximately 20% of fly ash is used to replace a part of cement in concrete production due to its pozzolanic and cementitious properties. Nowadays, it is necessary to develop new recycling technologies because over half of the fly ash is disposed of in dumping sites [25].

In this work, preactivated coal fly ash was hydrothermally treated for obtaining a solid powder enriched in NaA zeolite, and the zeolitized product was treated by ionic exchange to get the Cd ions as the counterbalancing cations for the anionic zeolite framework. The Cd-containing product was incorporated in Portland cement mortars to analyze its influence on the mortar textural properties. The flexural and compression strengths at 28 days were measured, and finally leaching tests of the heavy metal were performed to verify the viability of this process for Cd^{2+} immobilization in cement matrices.

Materials and methods

Fly ash and zeolite A synthesis

A fly ash from the thermoelectric power station at San Nicolás, Buenos Aires, Argentina, was used. According to the XRD analysis, the fly ash was composed by mullite ($Al_{4.52}Si_{1.48}O_{9.74}$) 17.2 wt%, Quartz ($SiO_2$) 5.5 wt%, Hematite ($Fe_2O_3$) 1.5 wt%, Calcite ($CaCO_3$) 1.6 wt%, and an amorphous phase, 74.2 wt% [26]. For this study, particles with a size fraction between 60 and 100 µm were selected by sieving.

Prior to the hydrothermal synthesis, the fly ash was activated by alkaline fusion using 50 wt% Na_2CO_3, according to the methodology described in [15]. Before heat treatment, the ash/carbonate mixture was sonicated. After 5 min of mixing, the solids were calcined under static conditions at 800 °C for 12 h. Pretreatment conditions, synthesis mixture compositions and maximum conversion in zeolite A are detailed in Table 1.

The alkali-activated ash was placed in contact with the synthesis mixture in a 250-mL polypropylene reactor. The reaction mixture was prepared by mixing appropriate amounts of NaOH (Carlo Erba p.a.) and deionized water. To obtain NaA zeolite as the main product, $NaAlO_2$ commercial solution (36.5% Al_2O_3, 29.6% Na_2O, 33.9% H_2O) was added as extra aluminum source. The starting mixture composition is detailed in Table 1. The sample was mixed with a magnetic stirrer for 30 min, aged at room temperature for 48 h, and placed in a conventional air oven at 100 °C. The reaction was carried out for 5 h to obtain the maximum conversion towards NaA [26]. The solid product obtained was washed and dried in a conventional air oven at 110 °C. The product obtained after 5 h of reaction time contained 65% of A zeolite, 22–27% of amorphous phase and a small fraction of other crystalline compounds (Table 1).

Physicochemical characterization

The structural characterization of crystalline materials (starting fly ash and the one resulting from hydrothermal synthesis) was carried out by XRD. The diffraction patterns were obtained in a PANalytical X´Pert PRO 3373/00 (40 kV, 40 mA, Cu Kα by Ni filter, step width 0.02°). The types of zeolite and other crystalline phases obtained were determined by comparing diffraction profiles with published data [27]. The Rietveld method [28] and the program "FULLPROF" [29] were used for the quantitative determination of the crystalline components (Table 1). Scanning electron microscopy (SEM) imaging and energy-dispersive X-ray (EDX) mapping were done using a Philips 505 microscope equipped with an EDX spectrometer. The specific areas corresponding to fly ash and zeolitized fly ash (ZFA) were estimated using the controlled humidity method, and IRAM 1624 was applied for density determination. Compared to coal fly ash, the product containing zeolite A resulted slightly denser and more hydrophilic than coal fly ash (Table 2).

After the synthesis, SEM micrographs (not included) corresponding to ZFA showed rounded particles about 2–50 µm in size. The spheres presented a surface fully covered by cubic crystals (typical morphology of NaA) of 3–5 µm of arista.

Table 1 Pretreatments, synthesis mixture compositions and maximum conversion in zeolite A

Zeolitized fly ash	Pretreatment		Activation solution (g)			NaA conversion (%)[a]	
	Calcination (h)	Na_2CO_3 (wt%)	H_2O	Al_2O_3	Na_2O	Time (h)	%
ZFA	12	50	88.8	0.438	3.10	5	65

[a]Estimated by XRD analysis. The product also contained 1.0% of low carnegieite, 2.2% of nepheline, 4.6% of hydroxysodalite, and around 22–27% of amorphous fraction

Table 2 Physical properties of fly ash and zeolitized fly ash (ZFA)

Sample	Density (g cm^{-3})	Specific surface (m^2 g^{-1})
Fly ash (FA)	2.20	25
Zeolitized fly ash (ZFA)	2.35	306

Table 3 Chemical analysis of FA, ZFA and Portland cement (wt%)

Compound	FA	ZFA	Portland cement
SiO_2	62.8	43.6	21.51
Al_2O_3	27.4	31.3	3.37
Na_2O	0.8	19.7	0.07
K_2O	0.7	–	1.01
CaO	1.8	2.3	64.78
MgO	–	1.2	0.77
TiO_2	1.4	0.5	–
Fe_2O_3	3.4	1.4	3.54
SO_3	–	–	2.21
Loss on ignition	–	–	2.44
Insoluble residue	–	–	0.54
Na_2O_{eq}	–	–	0.73
Other compounds	1.7	–	–

Cation exchange procedure

The cadmium-exchanged ZFA (Cd-ZFA) was obtained by contacting, under stirring, 3 g of ZFA with 1 L of solution containing 130 mg/L of Cd^{2+}. The solution was obtained by dissolving $CdCl_2 \bullet H_2O$ (Biopack, p.a.) in demineralized water. The pH was adjusted at 5.4 to avoid cadmium hydroxide precipitation; the contact time was 150 min. Samples of the suspension were collected at predetermined times and the liquid was separated from the solid by filtration. The solid phases were oven-dried at 110 C. The concentration of cadmium in the starting and remaining liquid phases was determined by atomic absorption spectroscopy (AAS) [30].

Cement mortar preparation and mechanical tests

Ordinary Portland cement (CPN50 type) and natural siliceous sand were used, the water/cement/sand ratios being 0.40:1:3. Considering the effects of mineral additions on the water demand, a naphthalene-based superplasticizer was incorporated to obtain workable mixtures without affecting the mixture proportions. Table 3 shows the EDX analysis of FA, ZFA, and Portland cement. Considering FA, the semi-quantitative SiO_2/Al_2O_3 molar ratio = 3.87 indicated that an extra source of alumina should be used for adjusting the batch synthesis composition to the molar ratios appropriate for obtaining NaA. It was observed that the SiO_2/Al_2O_3 ratio decreased in ZFA due to NaA crystallization (theoretical SiO_2/Al_2O_3 ratio in A zeolite is 2) (Table 3).

As shown in Table 3, the cement composition corresponds to an ordinary Portland cement. This cement was used instead of other types of cements (i.e., those incorporating calcareous filler or other mineral additions such as blast furnace slags) to avoid interactions with the studied FA and ZFA.

Two series of mortars incorporating different contents of FA (MFA5, MFA10, and MFA20) or ZFA (MZFA5, MZFA10, and MZFA20) as cement replacement (5, 10, and 20 wt%) were prepared. In addition, a reference mortar without mineral addition (MP) was also made.

Fresh mortars were characterized by the slump (using a height cone of 150 mm with the same geometric proportions as the Abrams cone) and unit weight (UW). Two sets of samples were cast: prisms of $40 \times 40 \times 160$ $mm^3$for flexural and compression strength measurements, and prisms of $30 \times 30 \times 220$ mm^3 to evaluate the drying shrinkage. The specimens were compacted by external vibration, selecting the time of vibration in agreement with the measured slump. The samples were removed from the molds after 1 day.

The compression and flexural strengths were evaluated after 7, 28, and 90 days. In this case, mortars were cured in water at 23 °C until test age. For drying shrinkage measurements, the mortars were cured in water at 23 °C for 8 days and then exposed to dry room air conditions (22 °C and 55% HR) for 6 months.

The crystalline phases were characterized by XRD as is described in "Cement mortar preparation and mechanical tests". In case of mortar structure analyses, the studied samples were collected from the exposed area obtained after mortar fracture.

To evaluate the ZFA capacity for heavy metal immobilization, an additional series of three cement pastes was prepared: a reference paste (PR) using a water/cement ratio 0.40 and two pastes incorporating 10% of cadmium-exchanged ZFA (PCd-ZFA10) or zeolitized fly ash (PZFA10) as cement replacement. Cement pastes instead of cement mortars were selected for avoiding sand interference in SEM observations. Prisms $30 \times 30 \times 220$ mm^3 in size were cast; the samples were removed from the molds after 1 day and cured in water at 23 °C up to the age of testing. For comparison with the mortar series, flexural and compression tests were performed at 28 days. SEM analyses and a leaching test were also done using the broken material. All tests were carried out in triplicate, and the results were averaged.

Leaching test

The leaching test was performed on PCd-ZFA10 following US EPA standard method 1311. The extraction solution was

prepared using 5.7 cm^3 of glacial CH_3CH_2OOH dissolved in distilled water up to 1 L volume. The paste was ground, and the fraction less than 1 mm was selected. The sample was put in contact with the extraction fluid, and the mixture was transferred to a glass container and submitted to stirring in a rotary shaker at 30 rpm for 18 h. Cd^{2+} in the remaining liquid was determined by AAS. Cd^{2+} in the curing water was also measured to evaluate the possible occurrence of cadmium leaching during the curing process [31]. The test was carried out in triplicate and the results were averaged.

Results and discussion

Properties of fresh mortars

The properties of fresh mortars are listed in Table 4. The content of chemical admixture was varied to achieve enough workability without modifying the water content. As expected, the superplasticizer requirement increases in MFA and mainly in MZFA mortars as the zeolite addition content increases. The greater water and superplasticizer demand of MZFA can be associated with the very high specific surface (see Table 2) and also with the hydrophilic nature of zeolite A crystals. Some reduction can also be seen in the unit weight of MZFA mortars, which can be attributed to a decrease in compactness.

Table 4 Fresh mortar properties

Mortar	Slump (mm)	Superplasticizer (wt%)	UW (kg m^{-3})
MP	30	0.6	2200
MFA5	30	1.1	2200
MFA10	55	1.5	2220
MFA20	40	1.8	2160
MZFA5	10	1.1	2040
MZFA10	10	1.5	2150
MZFA20	10	2.6	2130

Mechanical tests

The evolution of flexural and compression strengths up to 90 days is shown in Table 5. As expected, the strength increases with time, with the strength gain being greater in the case of MFA mortars. MZFA mortars show lower values than MFA, which is attributed to a lower pozzolanic activity of MZFA and less compactness of these mortars. A comparison of the flexural/compressive strength ratios (see Table 5) shows that they decrease as the strength increases, as is well known. The lower values correspond to the reference mortar (without mineral additions), which can be explained considering that the pozzolanic reactions consume calcium hydroxide improving the transition zone properties and then the tensile capacity.

Figure 1 presents the strength results as relative values referred to the results obtained at 28 days. The greater increase in the strength occurs between 7 and 90 days in the case of MFA mortars, which is more evident as the FA content increases. The strength evolution is smaller in MZFA mortars; it is possible that the more crystalline structure of ZFA will lead to a lower pozzolanic activity. The relative values are not so different than those observed in the reference mortar without additions.

From Table 5 it can be seen that MZFA mortars show lower strengths than the reference or MFA mortars; however, it must be emphasized that a compressive strength close to 40 MPa is compatible with many applications. From a practical point of view, the main advantage of ZFA addition can be associated with its ability to fix heavy metals (see "Cadmium uptake"). In these mortars, ZFA contents up to near 100 kg m^{-3} of mortar were incorporated.

Table 6 presents the mechanical properties measured after 28 days of moist curing on the cement pastes that were prepared to evaluate ZFA ability to immobilize heavy metals. The relative values among PR, PZFA10 and PCd-ZFA10 strengths are comparable with those found in the series of mortars. It can be seen that the compressive strength of PCd-ZFA10 (28.0 MPa) is much lower than 40 MPa. However, it must be noted that these small samples of cement pastes

Table 5 Evolution of compressive and flexural strengths in mortars

Sample	Flexural strength (MPa)			Compressive strength (MPa)			Flexural/compressive strength ratio (%)		
	7 days	28 days	90 days	7 days	28 days	90 days	7 days	28 days	90 days
MP	6.5	8.4	9.1	44.6	61.1	73.01	15	14	12
MZFA5	5.4	6.5	6.6	28.9	38.3	40.61	19	17	16
MZFA10	5.1	6.6	6.9	27.7	38.4	43.1	18	17	16
MZFA20	5.2	5.8	5.7	24.2	28.9	36.5	21	20	16
MFA5	5.8	7.2	7.8	34.4	46.3	60.2	17	16	13
MFA10	5.2	6.6	7.9	31.1	45.8	59.3	17	14	13
MFA20	4.3	6.7	7.1	23.1	36.5	50.0	19	18	14

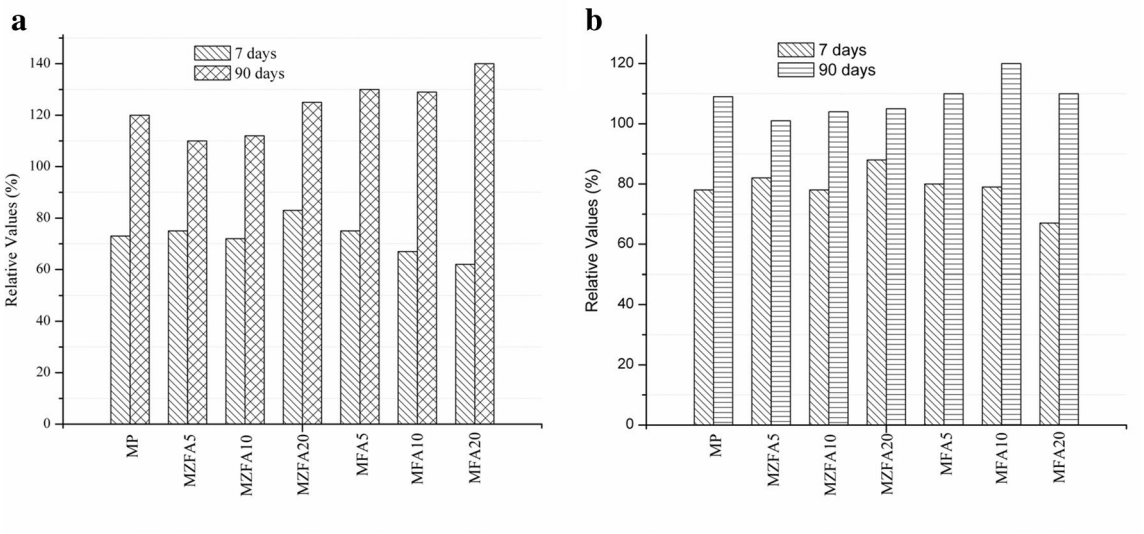

Fig. 1 Relative values of compressive (left) and bending (right) strength as a percentage of that measured at 28 days

Table 6 Mechanical properties of cement pastes

Paste	Flexural strength (MPa)	Compressive strength (MPa)	Flexural/compressive strength ratio (%)
PR	8.0	61.6	13
PZFA10	4.2	46.6	9
PCd-ZFA10	2.8	28.0	10

were prepared to evaluate the metal immobilization capacity corresponding to ZFA, not to evaluate the samples strength capacity.

Drying shrinkage

For practical applications, drying shrinkage is an important parameter related to the durability and susceptibility to cracking of Portland cement-based materials. As dimensional instability increases, greater possibilities of cracking appear when the material is restricted in its movements. The increases in water requirement due to the incorporation of mineral additions motivate the study of this property.

Figure 2 shows the evolution of drying shrinkage corresponding to the series of mortars. After moist curing, the specimens were exposed to dry room air conditions (RH 55%, 23 °C) for 6 months. As expected, the reference mortar (MP) has low values of drying shrinkage. MZFA20 clearly shows a great increase in shrinkage. This fact can be associated with both the increase in superplasticizer demand and the reduction of the mixture workability. Those factors promote a low compaction that was revealed by the low strength values obtained (Table 5). However, although the values of

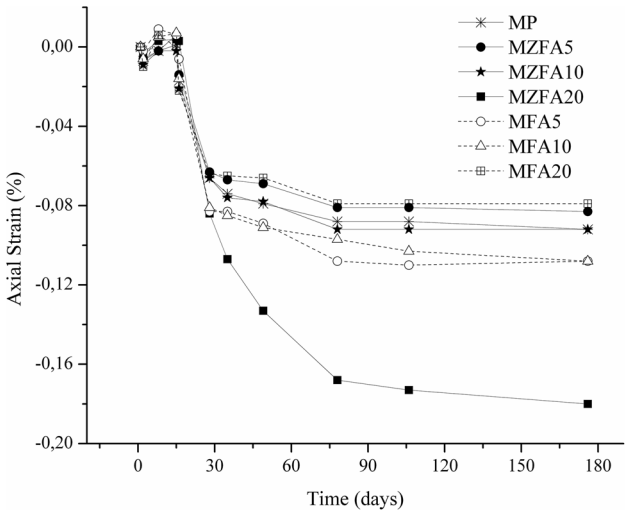

Fig. 2 Evolution of drying shrinkage

MZFA5 and MZFA10 are higher than those of MFA5 and MFA10, the differences are not significant (order variation of 0.02). Thus, it can be concluded that with up to 10% of ZFA incorporation as cement replacement there were not drastic changes in dimensional instability compared with fly ash mortars.

Microstructure

The microstructural morphology of the fractured mortars cured in water at 23 °C for 8 days and then exposed to room air conditions (22 °C and 55% RH) for 6 months was determined by SEM.

Figure 3 shows the reference mortar (MP), MFA20 and MZFA20 fracture areas. SEM images depict a typical microstructure of cement mortar mainly consisting of calcium silicate hydrates (C–S–H fibrous or reticular phases) in which fine and long needle-shaped ettringite crystals are embedded (Fig. 3a), crystals of sheet-shaped calcium hydroxide (portlandite, Fig. 3b) are also observed.

The MFA20 image (Fig. 3c) evidences the smooth spherical fly ash particles included in the C–S–H phase as well as the presence of small crystals of trigonal calcium carbonate (Fig. 3d). For MZFA20, as is shown in Fig. 3e, f, the microstructure of the fracture area appears quite different from those corresponding to MP and MFA20. In Fig. 3e, the presence of rounded ZFA particles is clearly observed, and ettringite crystals surrounding the ZFA particles are also

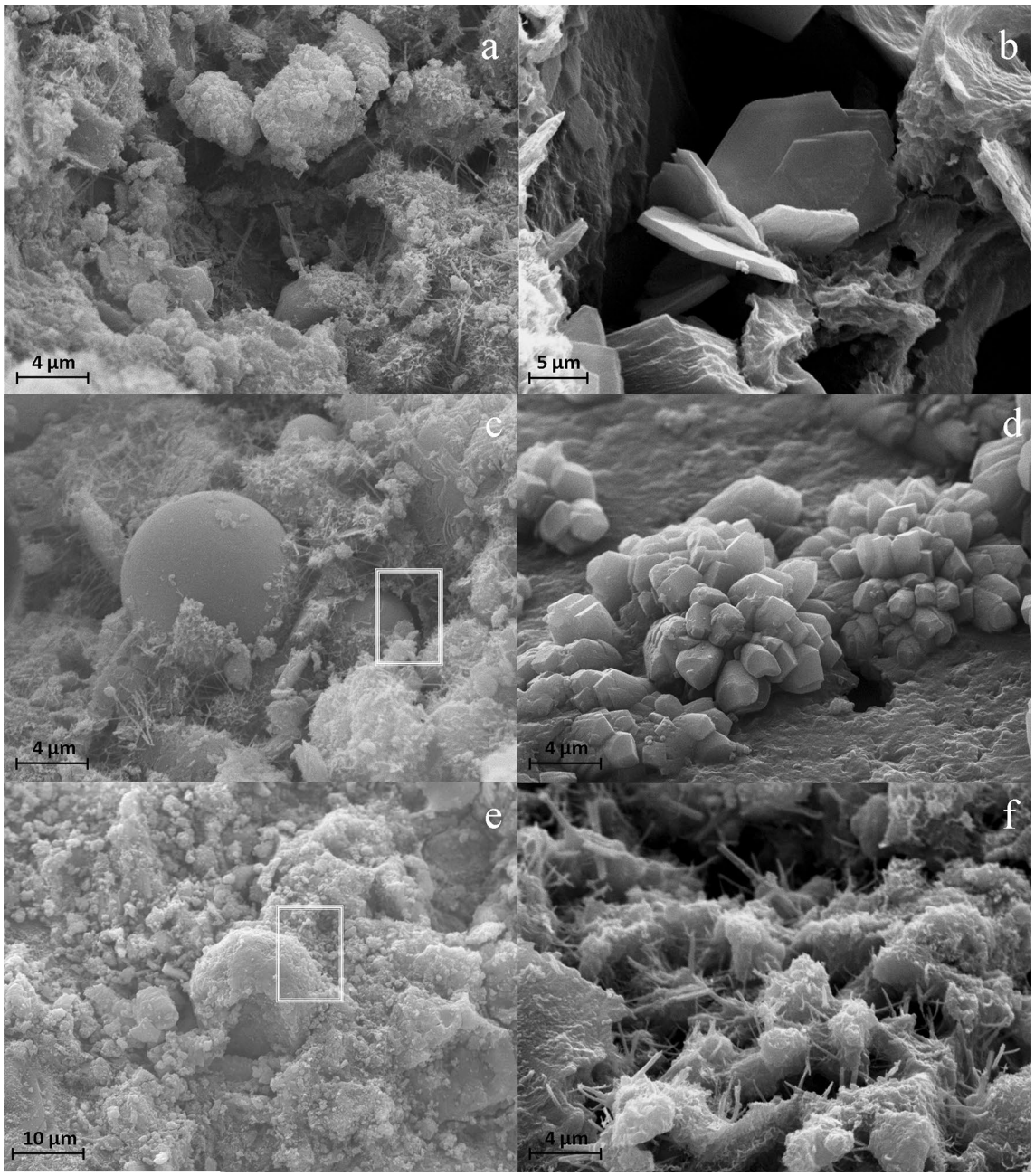

Fig. 3 SEM images of reference mortar microstructure, MFA20 and MZFA20 fractured mortars. **a** A typical structure containing calcium hydrate phases with fine and long needle-shaped ettringite, **b** sheet-shaped calcium hydroxide. Interfaces are marked with white squares in **c** and **d** for MFA20 and MZFA20, respectively. **e** Traces of calcite in MFA20. **f** Ettringite crystals are present as short and thick needles in MZFA20

detected. Nevertheless, in this sample the ettringite crystals are thicker and shorter than those found in samples MP and MFA20 (Fig. 3f). Recent studies have reported the influence of superplasticizer addition on the crystal size, morphology, and amount of ettringite crystals formed [32]. In the present analysis, the increased amount of naphthalene-based superplasticizer incorporated into MZFA20 (2.6 wt%) to enhance workability could modify ettringite crystallization. Furthermore, calcite formation is clearly observed when the ash particles are zeolitized in MZFA20 sample (Fig. 3).

Other differences have been found when MFA and MZFA particle–cement paste interfaces are compared. In mortars containing FA, SEM images corresponding to the fracture area show smooth fly ash particles almost free of hydration products (Fig. 3c), indicating that hydration products are slightly adhered to the fly ash surface. On the contrary, SEM images of MZFA fractured mortars show the zeolitized fly ash particles densely covered by hydration products (Fig. 3e).

Figure 4 shows XRD analyses of samples taken from MP, MZFA20 and MFA20. The presence of C–S–H phase (pdf# 10-0374) and quartz (pdf# 03-0419) was detected in all samples. The high concentration of natural sand in the mortars (1:3 cement/sand ratio) justifies the huge intensity of peaks corresponding to quartz.

Although ettringite crystals appeared in the SEM images, their peaks (pdf# 72-0646) are absent in all XRD patterns. Indeed, very low amounts of crystals are formed during curing, and their dispersion in the cement matrix could hinder the detection of ettringite in the X-ray analysis. Furthermore, ettringite could have been consumed by the reaction with calcium hydroaluminates to form hydrosulphoaluminate phases during cement hydration.

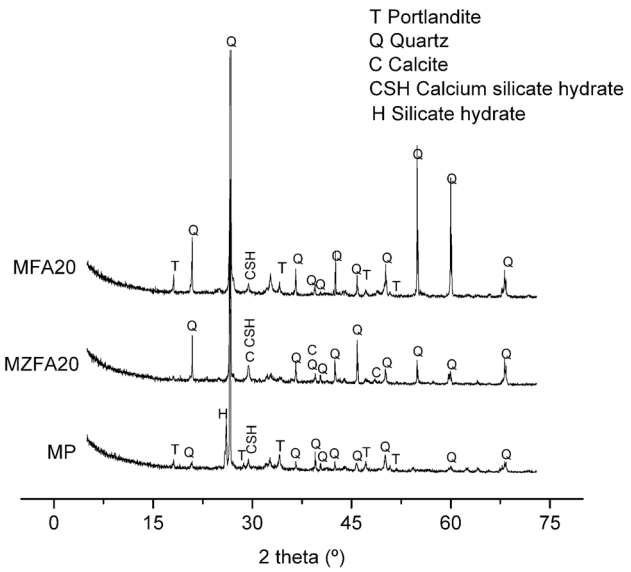

Fig. 4 X-ray diffraction patterns of MP and MZFA20

The calcium hydroxide crystals (portlandite, pdf# 78-0315) are present in the reference mortar even after 6 months of exposure to dry room air conditions (22 °C and 55% HR). However, portlandite is not observed in the zeolite-containing sample (MZFA20), and a new phase like calcium carbonate (calcite, pdf# 86-2334) was detected. This was expected because the mortars remained outdoors and unprotected against carbonation and the MZFA20 specimens probably have the greatest porosity (see strength and drying shrinkage measurements).

The peaks corresponding to mullite and quartz present in the original fly ash and the diffraction maxima corresponding to NaA zeolite are not found in the XRD patterns of MFA20 and MZFA20, respectively. These results are consistent with the low content of these minerals in the prepared mortars. The peaks for the FA sample (not shown) would mainly correspond to hematite (pdf# 73-0603), quartz and mullite (pdf# 79-1457) [26]. Based on the same reasons, the signals for zeolite A (pdf # 89-8015) were absent in the X-ray diffraction pattern. The calculated zeolite A content in MZFA20 was about 3%.

Cadmium uptake

According to AAS analyses, the cation exchange procedure allowed the incorporation of 22 wt% of Cd in the ZFA material (Cd-ZFA). The uptake rate of Cd^{2+} using the zeolitized fly ash was measured at different times under the conditions described in 2.3. The Cd^{2+} cations were quickly removed at the beginning of the cation exchange process (85 wt% at 20 min). To maximize the Cd concentration in the zeolitized sample, the selected contact time duplicates the time needed to reach the beginning of the maximum plateau in the Cd uptake vs. time curve.

Figure 5 shows a SEM image of Cd-ZFA (Fig. 5a) and the corresponding SEM–EDX mapping image of Cd (Fig. 5b). The red dots indicating Cd are uniformly distributed on the external particle surface, where the zeolite crystals are situated. This result is consistent with the fact that, after cation exchange, cadmium cations counterbalance the negative charge of zeolite A framework.

Leaching test results

The leaching analysis was done using samples taken from the PCd-ZFA10 used previously in the mechanical strength test.

According to AAS results, Cd^{2+} was not detected in the curing water of PCd-ZFA10 paste in which the sample was 28 days immersed under static conditions. In the leaching test carried out on samples from PCd-ZFA10, Cd^{2+}

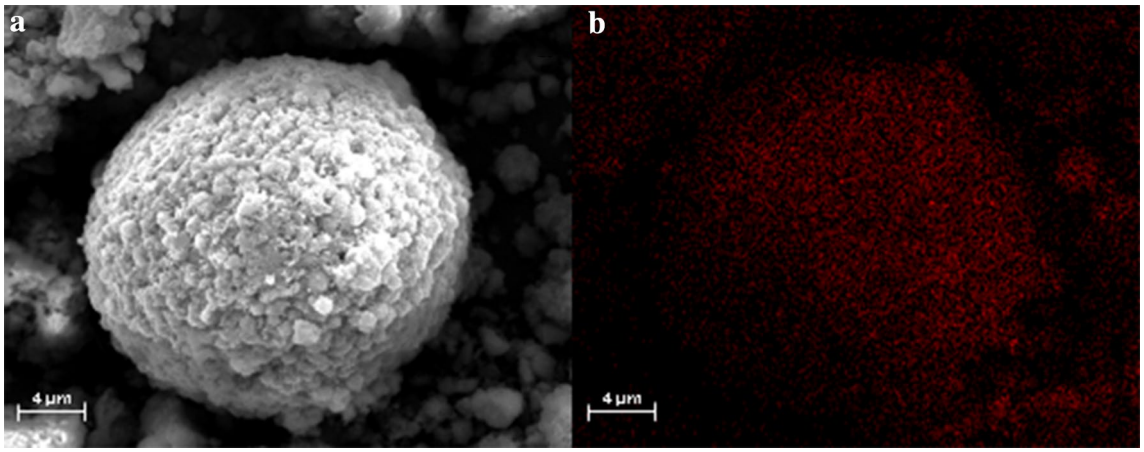

Fig. 5 SEM–EDX analyses of Cd-ZFA showing the same selected area in both pictures. **a** SEM image of Cd-ZFA. **b** Cd SEM–EDX mapping image corresponding to **a**

concentration in the liquid phase was 4×10^{-2} ppm. It is worthy to note that the last severe test conditions favored the cation leaching but the value was lower than the allowable limits (0.1 mg L^{-1}) established by Resolution 336/2003 of the Water Authority of Buenos Aires, Argentina.

SEM image of a Cd-ZFA particle included in ground PCd-ZFA10 after the leaching test and the corresponding Cd^{2+} SEM–EDX mapping image are shown in Fig. 6a, b. The EDX mapping shown in Fig. 6b would confirm that Cd^{2+} remains in the zeolitic structure after the leaching test.

Additionally, the SEM image of Fig. 6a shows the surface of Cd-exchanged zeolitized fly ash (Cd-ZFA) that is fully covered with hydration products. Zeolite cubic crystals cannot be seen and significant amounts of calcium carbonate crystals (calcite, Fig. 6c) were detected by EDX and XRD analyses (not shown). Also, irregular sheet-shaped structures corresponding to the hydrosulphoaluminate (C_4ASH_{12}) phase [33] appear due to the hydroalumination reaction (Fig. 6d). In this way, the incorporation of the Cd-exchanged zeolite in PCd-ZFA10 could enlarge calcite and hydroaluminate formation in capillary pores. This fact could contribute to the increase in paste density, improving the resistance to leaching [34].

Conclusions

A zeolite A-rich product containing about 65 wt% of NaA (ZFA) was successfully obtained by alkaline fusion treatment applied to fly ash (FA) discarded from a thermoelectric power plant. Portland cement mortars and pastes incorporating different contents of FA and ZFA were made. The microstructure characteristics, strength evolution, drying shrinkage, and leaching test results were analyzed.

As expected, increases in mortar strength between 7 and 90 days are greater as the FA content increases; strength evolution is smaller in ZFA mortars, which can be associated with a lower pozzolanic activity of ZFA particles. Although ZFA mortars show lower strengths than FA mortars, the obtained compressive strength is compatible with many usual applications.

The drying shrinkage increases as FA or ZFA content increases, the values being very high in the case of mortar with 20% of ZFA. Nevertheless, up to 10% of ZFA incorporation as cement replacement, the shrinkage is similar to that of FA mortars.

The high specific surface and the hydrophilic nature of ZFA increase the superplasticizer demand to maintain the workability. The increased addition of superplasticizer reduces ettringite formation and alters ettringite crystal morphology.

Fractured MZFA20 mortars show zeolitized fly ash particles strongly anchored inside the microstructure, the particle surfaces being densely covered by hydration products. Calcite and CSH crystal growth is enhanced in MZFA20 mortars.

The zeolitic material synthesized from the activated fly ash can remove Cd^{2+} from aqueous solutions.

The leaching test of the heavy metal indicated that in pastes of 0.40 water/cement ratio, using Cd-ZFA contents lower than 10 wt%, an effective immobilization of Cd^{2+} cations occurs. Also, the formation of new crystalline structures (hydrosulphoaluminate phase and increased calcite content) contributes to the increase in paste density, reducing cation leaching. The incorporation of Cd-ZFA in concrete and other Portland cement-based materials can be considered as a valid option for cadmium disposal.

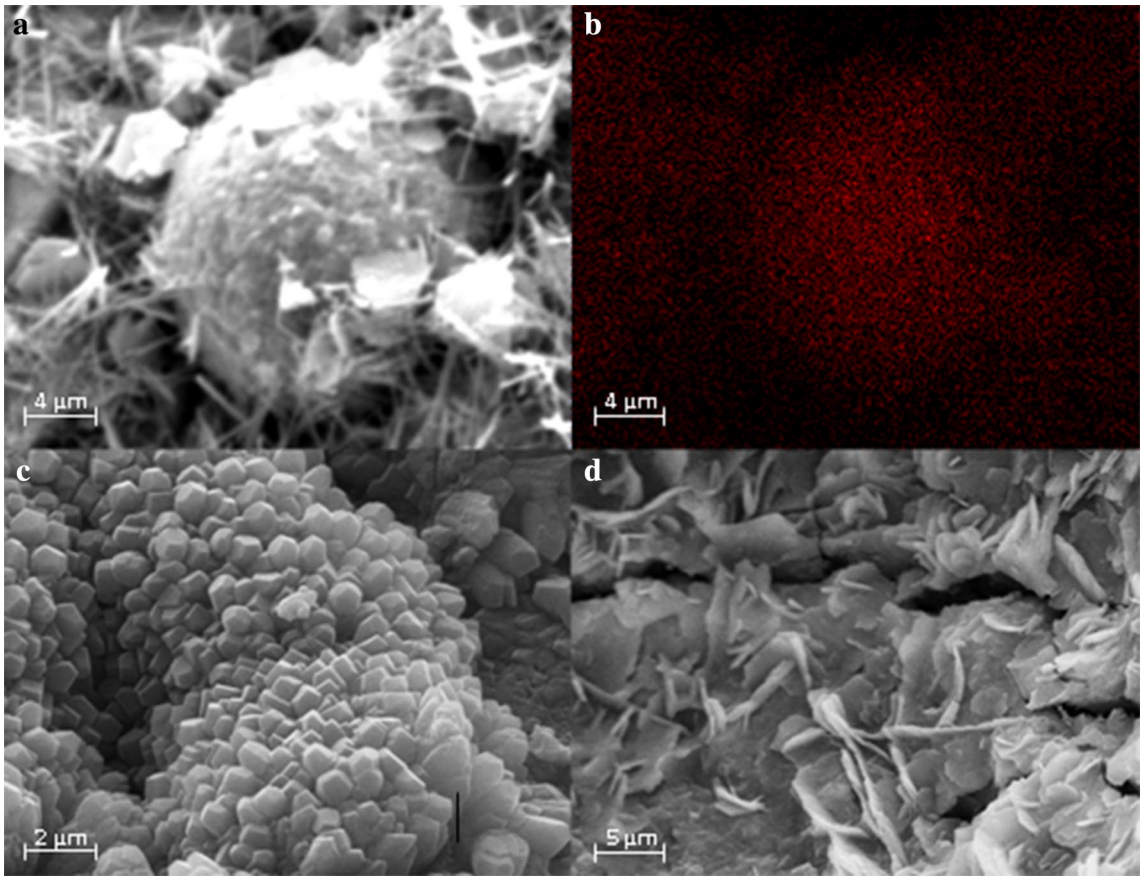

Fig. 6 PCd-ZFA10 paste after the leaching test. **a** SEM image of a Cd-ZFA particle dispersed in ground PCd-ZFA10 paste. **b** SEM–EDX mapping image of Cd. **c** High content of calcite in PCd-ZFA10 paste. **d** C_4ASH_{12} phase

Acknowledgements The authors are grateful to CONICET, CICPBA and UTN for supporting this research. The authors also thank Lic. G. Kürten and Lic. M. Theiller for performing the XRD and SEM–EDX experiments and Dr. N. Quaranta for providing the fly ash samples used in this work.

References

1. Fu F, Wang Q (2011) Removal of heavy metal ions from wastewaters, a review. J Environ Manage 92:407–418
2. Fosso-Kankeua E, Mittalb H, Waandersa F, SuprakasSinha R (2017) Thermodynamic properties and adsorption behaviour of hydrogel nanocomposites for cadmium removal from mine effluents. J Ind Eng Chem 48:151–161
3. Zhu X, Li J, Luo J, Jin Y, Zheng D (2017) Removal of cadmium (II) from aqueous solution by a new adsorbent of fluorhydroxyapatite composites. J Taiwan Inst Chem Eng 70:200–208
4. Bhanjana G, Dilbaghi N, Singhal NK, Kim K, Kumara S (2017) Copper oxide nanoblades as novel adsorbent material for cadmium removal. Ceram Int 43:6075–6081
5. Chen K, He J, Li Y, Cai X, Zhang K, Liu T, Hu Y, Lin D, Kong L, Liu J (2017) Removal of cadmium and lead ions from water by sulfonated magnetic nanoparticle adsorbents. J Colloid Interface Sci 494:307–316
6. Othman CS. Hamouz A, Estatie M, Saleh TA (2017) Removal of cadmium ions from wastewater by dithiocarbamate functionalized pyrrole based terpolymers. Sep Purif Technol 177:101–109
7. Snoussi Y, Abderrabba M, Sayari A (2016) Removal of cadmium from aqueous solutions by adsorption onto polyethylenimine-functionalized mesocellular silica foam: Equilibrium properties. J Taiwan Inst Chem Eng 66:372–378
8. Roushani M, Saedi Z, Baghelani YM (2017) Removal of cadmium ions from aqueous solutions using TMU-16-NH2 metal organic framework. Environ Nanotechnol Monit Manage 7:89–96
9. Hadjltaief HB, Sdiri A, Ltaief W, Ltaief W, Da Costa P, Galvez ME, Zina MB (2017) Efficient removal of cadmium and 2-chlorophenol in aqueous systems by natural clay: adsorption and photo-Fenton degradation processes. C R Chimie xxx:1–10
10. Wang H, Wang X, Ma J, Xia P, Zhao J (2017) Removal of cadmium (II) from aqueous solution: a comparative study of raw attapulgite clay and a reusable waste–struvite/attapulgite obtained from nutrient-rich wastewater. J Hazard Mater 329:66–76
11. Zahri NAM, Jamil SNAM, Abdullah LC, Huey SJ, Yaw TCS, Mobarekeh MN, Rapeia NSM (2017) Equilibrium and kinetic behavior on cadmium and lead removal by using synthetic polymer. J Water Process Eng 17:277–289
12. Meng Q, Chen H, Lin J, Lin Z, Sun J (2017) Zeolite A synthesized from alkaline assisted pre-activated halloysite for efficient heavy metal removal in polluted river water and industrial wastewater. J Environ Sci 56:254–262

13. Ltaief OO, Siffert S, Fourmentin S, Benzina M (2015) Synthesis of Faujasite type zeolite from low grade Tunisian clay for the removal of heavy metals from aqueous waste by batch process: Kinetic and equilibrium study. C R Chimie 18:1123–1133
14. Jamil TS, Ibrahim HS, Abd El-Maksoud IH, El-Wakeel ST (2010) Application of zeolite prepared from Egyptian kaolin for removal of heavy metals: I. Optimum conditions. Desalination 258:34–40
15. Gonzalez MR, Firpo N, Basaldella EI (2009) Materiales zeolíticos para purificación de aguas obtenidos a partir de catalizadores de cracking agotados. XVI Congreso Argentino de Catálisis, Buenos Aires
16. Jha VK, Nagae M, Matsuda M, Miyake M (2009) Zeolite formation from coal fly ash and heavy metal ion removal characteristics of thus- obtained Zeolite X in multi-metal systems. J Environ Manag 90:2507–2514
17. Querol X, Moreno N, Umana JC, Alastuey A, Hermandez E, López-Soler A, Plamera F (2002) Synthesis of zeolites from coal fly ash; an overview. Int J Coal Geol 50:413–423
18. Shawabkeh R, Al-Harahsheh A, Hami M, Khlaifat A (2004) Conversion of oil shale ash into zeolite for cadmium and lead removal from wastewater. Fuel 83:981–985
19. Belviso C, Cavalcante F, Fiore S (2010) Synthesis of zeolite from Italian coal fly ash: differences in crystallization temperature using seawater instead of distilled water. Waste Manage 30:839–847
20. Chen J, Lu X (2018) Synthesis and characterization of zeolites NaA and NaX from coal gangue. J Mater Cycles Waste 20:489–495
21. Wang CF, Li JS, Wang LJ, Sun XY (2008) Influence of NaOH concentrations on synthesis of pure-form zeolite A from fly ash using two stage method. J Hazard Mater 155:58–64
22. Cho H, Oh D, Kim K (2005) A study on removal characteristics of heavy metal from aqueous solution by fly ash. J Hazard Mater B 127:187–195
23. Ilic M, Cheeseman C, Sollars C, Knight J (2003) Mineralogy and microstructure of sintered lignite coal fly ash. Fuel 82:331–336
24. Nihon FK, Kankyogijyutsu K (2005) Coal ash handbook. Tokyo
25. Shigemoto N, Hayashi H, Miyaura K (1993) Selective formation of NaX, zeolite from coal fly ash by fusion with sodium hydroxide prior to hydrothermal reaction. J Mater Sci 28:4781–4786
26. Monzón JD, Pereyra AM, Conconi MS, Basaldella EI (2017) Phase transformations during the zeolitization of fly ashes. J Environ Chem Eng 5(2):1548–1553
27. Breck DW (1974) Zeolite molecular sieves. Wiley, New York
28. Rietveld HM (1969) A profile refinement method for nuclear and magnetic structures. J Appl Crystal 2:65–71
29. Rodríguez-Carvajal J (2001) Recent developments of the program FULLPROF, in commission on powder diffraction (IUCr). Newsletter 26:12–19
30. Gonzalez MR, Pereyra AM, Torres Sanchez RM, Basaldella EI (2013) Chromium removal by zeolite-rich materials obtained from an exhausted FCC catalyst: influence of chromium incorporation on the sorbent structure. J Colloid Interf Sci 408:21–24
31. Gonzalez MR, Pereyra AM, Zerbino R, Basaldella EI (2015) Removal and cementitious immobilization of heavy metals: chromium capture by zeolite-hybridized materials obtained from spent fluid cracking catalysts. J Clean Prod 91:187–190
32. Shi C, Zhang G, He T, Li Y (2016) Effects of superplasticizers on the stability and morphology of ettringite. Constr Build Mat 112:261–266
33. Girskas G, Skripkiunas G (2017) The effect of synthetic zeolite on hardened cement paste microstructure and freeze-thaw durability of concrete. Constr Build Mater 142:117–127
34. Nagrockiene D, Girskas G, Skripkiunas G (2014) Cement freezing–thawing resistance of hardened cement paste with synthetic zeolite. Constr Build Mater 66:45–52